Journal of Solid State Chemistry **163,** 163–177 (2002)
doi:10.1006/jssc.2001.9389, available online at http://www.idealibrary.com on IDEAL®

Structural Investigation of Mixed Nitrided Galloaluminophosphates "AlGaPON" by EELS, XAS, and XPS Spectroscopies

S. Delsarte,*,[1] V. Serin,† A.-M. Flank,‡ F. Villain,§ and P. Grange*

*Catalyse et Chimie des Matériaux Divisés, Université catholique de Louvain, Croix du Sud 2/17, 1348 Louvain-la-Neuve, Belgique; †Centre d'Elaboration des Matériaux et d'Etudes Structurales (CEMES), 29, Rue Jeanne Marvig, BP 4347, 31055 Toulouse Cedex 4, France; ‡Laboratoire pour l'Utilisation du Rayonnement Electromagnétique (LURE), Centre Universitaire Paris-sud, BP 34, 91898 Orsay Cedex, France; and §Laboratoire de Chimie Inorganique et Matériaux Moléculaires, Université Pierre et Marie Curie, 4 Place Jussieu, 75252 Paris, France

Received April 9, 2001; in revised form August 29, 2001; accepted September 7, 2001

Amorphous nitrided galloaluminophosphates "AlGaPON" catalysts with nitrogen contents varying from 0 to 23.3 wt% N were obtained by nitriding an $Al_{0.5}Ga_{0.5}PO_4$ precursor under ammonia flow at 750°C in a tubular furnace. The structural changes induced by this treatment were investigated by electron energy loss spectroscopy (EELS), X-ray absorption spectroscopy (XAS), and X-ray photoelecton spectroscopy (XPS). XANES and XPS results indicate that the first-coordination spheres of P, Ga, and Al atoms are modified by nitridation. In particular, the comparison of the P XANES spectra recorded on "AlGaPON" and on a PON phosphorus oxynitride (reference of mixed PO_2N_2 tetrahedra) reveals that mainly PO_2N_2 tetrahedra are present in highly nitrided samples. Moreover, the replacement of oxygen by nitrogen probably concerned P–O–Ga bonds rather than P–O–Al. EELS investigation reveals that the precursor is homogeneous at the used probe scale, but indicates that nitridation is accompanied by a loss of homogeneity of the material.

Key Words: **AlGaPON; oxynitrides; basic catalysts; EELS; XAS; XPS.**

I. INTRODUCTION

Various types of metal phosphates, in amorphous or crystalline form, are used as acid and base catalysts (1). It is well known that their acid–base properties can be adjusted by changing the preparation and activation conditions (2–4). Recently, another way to modify the surface acid–base properties of phosphates was proposed: the nitridation under ammonia flow at moderate temperatures (600–800°C) (5). The reaction, only possible with amorphous solids (6), allows replacement of three oxygen atoms by two nitrogen atoms in the phosphate network and obtaining nitrogen contents as high as 20 wt%. The reaction is carried out between flowing pure ammonia and the precursor placed in the isothermal region of a tubular furnace.

The considerable changes induced by this treatment on the phosphates acid–base properties were first demonstrated on two families of amorphous catalysts: the nitrided zirconophosphates "ZrPON" (7–10) and the nitrided aluminophosphates "AlPON" (11, 12). More recently, we developed a new family of mixed nitrided galloaluminophosphates "AlGaPON". Those solids are synthesized by ammonolysis of an amorphous $Al_{0.5}Ga_{0.5}PO_4$ precursor (13). This precursor has a marked acid character due to the presense of surface Brönsted and Lewis acid sites. Pyridine adsorption experiments carried out on the precursor indicated that the presence of Brönsted acid sites was mainly due to the existence of surface P–OH species, while the presence of Lewis acid sites was attributed to coordinatively unsaturated Al^{3+} and Ga^{3+} ions (14, 15). Incorporation of nitrogen in the phosphate network leads to the decrease of the number of acid sites (14) and to the appearance of weak surface basic sites (14, 16, 17). Those results demonstrate that the acid–base properties of AlGaPONs can be tailored by adjusting their nitrogen content, which is very valuable for applications in heterogeneous catalysis.

The AlGaPONs were already successfully used as catalysts of the Knoevenagel condensation between benzaldehyde and malononitrile, a reaction widely described in the literature (18) and typically catalysed by bases. The catalytic activities obtained for the oxynitrides were much larger than those for the corresponding oxide, indicating the major influence of nitrogen on the basic properties (14, 16). Besides, the AlGaPON catalysts were also successfully used as support for platinum in the dehydrogenation of isobutane to isobutene (19, 20).

Several publications have already been dedicated to the structural study of AlPON catalysts. Due to the amorphous nature of these catalysts, classical X-ray diffraction experiments could not be used to study their structure. Other approaches were chosen: ^{27}Al and ^{31}P NMR (nuclear

[1] To whom correspondence should be addressed. Fax: 00 32 10 47 36 49. E-mail: gueguenerw@hotmail.com.

0022-4596/02 $35.00

magnetic resonance) (6, 21, 22), XPS (X-ray photoelectron spectroscopy) (23–25), and DRIFTS (12, 23–27) (diffuse reflectance Fourier transform infrared dpectroscopy) spectroscopic data were combined with ab initio SCF calculations on model systems (28). Those studies revealed a preferential nitridation of phosphorus atoms as compared to aluminium atoms. Such a preference was expected (29) since the bond strength of P–N is slightly greater than that of P–O, whereas Al–O bonds are stronger than their nitrogen analog (bond strengths (kJ/mol): P–N, 617; P–O, 597; Al–N, 297; Al–O, 512) (30).

In 1998, Benitez *et al.* (24) proposed that nitridation of the $AlPO_4$ precursor induced the segregation of an Al_2O_3-type phase and the appearance of –N=P–N cyclic arrangements. In their opinion, nitrogen was not incorporated in the first shell of aluminium. They later extended this model by suggesting that the existence of a surface AlON phase should be considered (25) and that P–N–Al bonds were formed when the nitrogen content increases over a certain value (typically 15–20 wt%), linking together the metaphosphate-like rings (28).

The existence of a cyclic ring structure with alternating P–N–P bonds in AlPON is supported by the presence in the DRIFTS spectra of a broad and weak band around 2700 cm^{-1} that can be associated to hydroxyl groups linked to P in P–N–P bonds in cyclic phosphonitrilates (24).

The changes induced by nitridation on the structure of amorphous $Al_{0.5}Ga_{0.5}PO_4$ phosphates had not yet been studied. The aim of this study was to answer two fundamental questions:

1. Is nitrogen incorporated in the first-coordination sphere of P, Ga, and Al atoms?

2. Are some of those elements nitrided preferentially?

To answer these questions, XPS, XAS, and EELS spectroscopic studies were carried out on five samples with identical Al/P and (Al + Ga)/P atomic ratios, but with different O/N ratios.

The EELS spectroscopy was also used to perform elemental chemical analysis of the samples at the nanometer scale to assess the homogeneity of the $Al_{0.5}Ga_{0.5}PO_4$ precursor and to verify whether or not nitridation caused a loss of homogeneity of the material.

II. EXPERIMENTAL

II.1. Materials

The high surface area, amorphous $Al_{0.5}Ga_{0.5}PO_4$ precursor was synthesized by a process developed by Kearby (31) for aluminophosphates and adapted for the "(Al, Ga)PO" compositions (13). A solution of adequate amounts of Ga^{3+}, Al^{3+}, and H_3PO_4 (2M) (P/(Ga + Al) and Ga/Al atomic ratios of 1) was cooled at 0°C in a dry ice–alcohol bath. Then, a large excess of propylene oxide was slowly added under vigorous stirring. After some hours at room temperature, a translucent gel was produced. The gel was washed with isopropanol and dried at 110°C. The resulting powder was sieved ($Ø < 100$ μm) and calcined in air at 650°C.

The precursor, placed in the isothermal region of a tubular furnace, was activated under ammonia flow (30 L h^{-1}) at 750°C. Various nitrogen contents were obtained by modifying the time of nitridation from 3 to 89 h. At the end of the activation process, the samples were cooled down to room temperature under pure and dry nitrogen flow.

The crystalline $Al_{0.5}Ga_{0.5}PO_4$ phosphate was obtained by heating (10°C/min) the amorphous precursor in a muffle furnace for 10 h at 1300°C.The resulting material is well crystallized and the X-ray diffraction (XRD) spectra present peaks at positions intermediate between those of orthorhombic $AlPO_4$ and $GaPO_4$.

Details about the synthesis and the structure of the $Na_3AlP_3O_9N$ (reference for PO_3N tetrahedra) and the β-cristobalite PON (reference for PO_2N_2 tetrahedra) phosphorus oxynitrides can be found in Refs. (6, 32–34 and 35, 36), respectively. The composition of those samples was determined by chemical analysis, the nitrogen content being determined by the Grekov method detailed hereafter. The existence of only one crystalline phase was checked by XRD (X-ray diffraction).

II.2. Textural Analysis

The surface areas of the samples were measured by the single-point BET method in a Micromeritics (Flowsorb II 2300) apparatus, after 20 min of degassification at 250°C.

Porosity measurements by the BET method were realized in a Micromeritics (ASAP 2000) apparatus. The adsorption isotherms were recorded at -196°C in the $10^{-6} < P/P_0 < 0.99$ pressure range after degassification of the samples (100 mg) under vacuum (0.1 Pa) at 200°C for 1 night.

II.3. Nitrogen Analysis by the Grekov Method

The total nitrogen content of the "AlGaPON" samples was determined by titration with a sulfuric acid solution of the ammonia liberated in alkaline digestion at 400°C with melted KOH (37).

II.4. Eelectron Energy Loss Spectroscopy

EELS experiments were conducted on a Philips CM20 transmission electron microscope equipped with a LaB6 source and a Gatan PEELS 666 parallel energy loss spectrometer. Experiments were performed either at 100 kV (giving a resultant energy resolution of ca. 1.2 eV) for ELNES (energy loss near edge structure) investigation or at 200 kV for the quantitative analysis. Spectra were collected in diffraction mode with a probe diameter in the range from about 20 to 100 nm using convergence and collection angles

of 7 and 3 mrd, respectively. This value of the collection angle lies well within the regime for dipole-allowed electronic transition. For TEM and EELS analysis, the powdery samples were ground and deposited on carbon microgrids.

EELS analysis was performed at N–K, O–K, Ga–$L_{2,3}$, Al–K, and P–K occurring at about 401, 532, 1115, 1560, and 2146 eV, respectively. Care was taken to use short enough recording times (a few seconds to 1 min from N–K to P–K edges) to obtain sufficient signal-to-noise ratios and to prevent radiation damage to samples.

The relative O/N, Al/P, and Al/Ga concentrations were determined by classical EELS quantitative analysis, as proposed for instance by Egerton (38). The accuracy was on the order of 10%.

All edges displayed hereafter have been processed for background subtraction, using a standard routine based on a power-law model for the pre-edge decay.

II.5. X-ray Absorption Spectroscopy

The X-ray photo-absorption experiments have been performed at Super ACO and DCI (LURE, Centre Universitaire Paris-Sud, Orsay, France).

Al and P spectra were recorded on the SA32 soft X-ray beamline using the two-crystals monochromator equipped with quartz (10–10) for Al–K edge and Ge(111) for P–K edge. The spectra were calibrated using an aluminium metallic foil for Al–K edge (1559 eV at the inflexion point) and ZnS for the P–K edge (2473 eV at the inflexion point of the S–K edge). The incident beam was monitored by measuring the total electron drain current of a Be or an Al foil located downstream the monochromator. The experimental resolution was of the order of 0.5 eV for Al–K and 0.7 eV for P–K.

The Al and P–K edges of AlGaPON were recorded using total electron yield (on samples mechanically pressed at room temperature on an indium foil, which avoids charging effects during measurements), while the Al and P spectra of AlPON were recorded using the transmission mode (on samples finely ground and deposited on thin polyurethane membranes). The transmitted beam was measured using an ionization chamber filled by a low pressure of air.

The Ga–K edges were measured on the EXAFS 13 station using the two-crystals monochromator equipped with Si(311). The spectra were calibrated using zinc metallic foil (9659 eV at the inflexion point). The experimental resolution was of the order of 2.5 eV and the measurements were done in transmission mode using ionization chambers filled with argon. The gas pressure in the chamber was adjusted to obtain currents of approximately 1.5 nA. The samples were mixed with cellulose and pressed in disks that were stuck between two X-ray transparent capton films. The XANES spectra were recorded at room temperature and the EXAFS ones at liquid nitrogen temperature.

II.6. X-ray Photoelectron Spectroscopy

Two different spectrometers, a SSI SSX-100/206 spectrometer and a VG ESCA-3MkII spectrometer, were used for the XPS experiments.

The VG ESCA-3MkII spectrometer is equipped with a Mg non-monochromatized X-ray anode source, a hemispherical analyzer, and a channel electron multiplier as a detection system. Details concerning this kind of spectrometer have been given previously (39, 40).

The sample powders were pressed into stainless steel troughs (8-mm diameter) and placed on a metallic cane. The samples were outgassed overnight at room temperature before introduction into the analysis chamber. The routine pressure of the analysis chamber was less than 10^{-8} Torr. The Mg non-monochromatized X-ray anode source was operated at 14 kV and 20 mA.

The SSI X-probe (SSX-100/206) of Fisons is a spectrometer consisting of a monochromatized microfocus Al X-ray source, an electron collection lens, a hemispherical analyzer, and a microchannel plate as a detector. Details concerning this kind of spectrometer have been given previously (41).

The sample powders were pressed into stainless steel troughs (4-mm diameter) and placed on an aluminium carousel. The samples were heated by a quartz lamp (maximum 120°C) three times for 15 min under vacuum. The heating periods were separated by 30-min pauses for outgassing. The samples were then outgassed overnight under vacuum and introduced into the analysis chamber. The residual pressure during the analysis remained between 1 and 5×10^{-9} Torr. The Al monochromatized X-ray source was operated at 10 kV. A low-energy flood gun (6 eV) with a Ni grid placed 3 mm above the samples was used to compensate for charging during measurements.

For each sample, a survey spectrum was recorded, followed by detailed scans of C_{1s}, O_{1s}, N_{1s}, Ga_{3p}, Al_{2p}, P_{2p}, Ga_{3d}, and finally C_{1s} again. Binding energies were calculated with respect to the C–(C,H) component of the C_{1s} adventitious carbon fixed at 284.8 eV. The spectra were decomposed with the least-squares fitting routine with a Gaussian/Lorentzian ratio of 85/15 and after subtraction of a nonlinear baseline. The atomic ratios were calculated from the relative intensities of the peaks recorded with the VG ESCA-3MkII spectrometer corrected by the Weng sensitivity factors (42).

III. RESULTS

III.A. Synthesis of "AlGaPON" Oxynitrides, Nitridation Parameters

The $Al_{0.5}Ga_{0.5}PO_4$ amorphous precursor was heated in flowing ammonia for various durations at 750°C. This treatment induces the progressive substitution of oxygen for

TABLE 1
Characteristics of the Oxide and Oxynitride AlGaPO(N) Powders

Sample	Composition	Nitridation time (h)	Weight nitrogen content (wt%)	Atomic nitrogen content (%)	Surface area (m^2/g)
AG9	$Al_{0.5}Ga_{0.5}PO_4$	—	—	—	240
AG9N2	$Al_{0.5}Ga_{0.5}PO_{3.22}N_{0.52}$	3	5.3	9.1	150
AG9N4	$Al_{0.5}Ga_{0.5}PO_{2.43}N_{1.04}$	8	11.0	19.0	160
AG9N5	$Al_{0.5}Ga_{0.5}PO_{1.81}N_{1.46}$	16	15.9	27.7	145
AG9N6	$Al_{0.5}Ga_{0.5}PO_{0.94}N_{2.04}$	89	23.3	41.0	170

nitrogen—3O/2N—for charge balance according to Eq. [1]:

$$Al_{0.5}Ga_{0.5}PO_4 + xNH_3 \rightarrow Al_{0.5}Ga_{0.5}PO_{(4-3x/2)}N_x + 3x/2\ H_2O\uparrow \quad [1]$$

The choice of experimental conditions for nitridation is conditioned by the Al/Ga ratio of the precursor (13). In all cases, however, the nitridation temperature cannot exceed 800°C; indeed at higher temperatures, a partial reduction of P^{5+} phosphorus atoms by ammonia with formation of volatile phosphines leads to phosphorus-deficient oxynitrides with the general formula $Al_{0.5}Ga_{0.5}P_{1-a}O_{4-(3sc+5a)/2}N_{sc}$.

The nitrogen content of the nitrided powders was determined by the Grekov method (37). The results are presented in Table 1. This table shows that the nitridation content of the samples increases with the time of nitridation. This evolution is illustrated in Fig. 1. As for the AlPON (6) and ZrPON (43) systems, the rate of nitrogen incorporation decreases when the nitrogen content increases, and the total nitrogen content tends toward a maximum of approximately 20 wt% N.

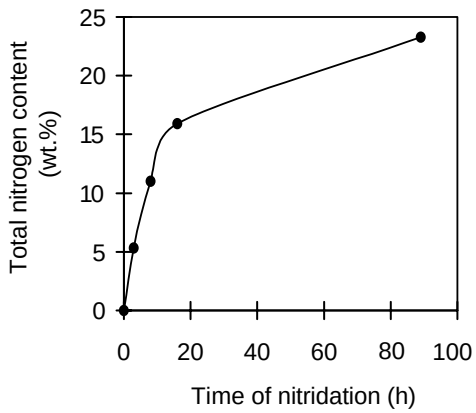

FIG. 1. Nitrogen enrichment as a function of time.

The compositions of the nitrided samples presented in Table 1 were established from the total nitrogen content of the samples. Indeed, it has been shown that the Al/Ga and (Al + Ga)/P ratios were maintained during nitridation at this temperature and that the weightloss recorded during nitridation corresponded to the replacement of three oxygen atoms by two nitrogen atoms (13). Besides, we verified that the O/N atomic ratio calculated for the AG9N5 sample ($O/N_{calculated} = 1.2$) was similar to the atomic ratio established from the chemical dosage of the O and N total content of the samples ($O/N_{experimental} = 1.1$) (LECO elemental analyzer equipped with a TC-346 program and an EF-400 oven).

III.B. Morphology and Texture

The mixed galloaluminophosphates obtained by the Kearby (31) method are highly divided X-ray amorphous white powders (13). Nitrogen adsorption and desorption isotherms recorded on those samples at -196°C present a hysteresis loop, characteristic of type IV isotherms, which indicates the prevalence of mesopores (44).

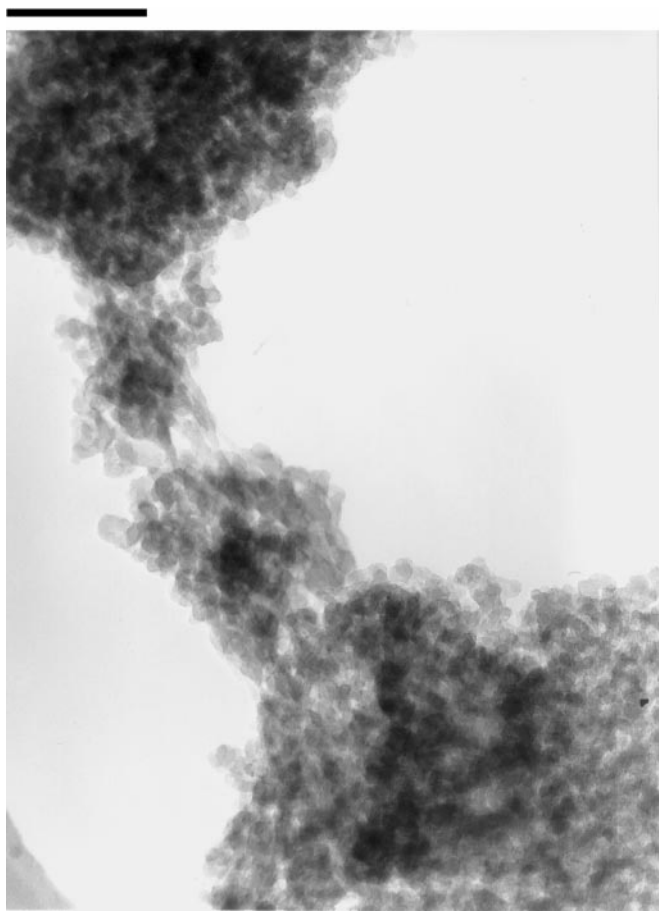

FIG. 2. TEM micrograph of the AG9 precursor (the length of the reference line is equivalent to 100 nm).

FIG. 3. TEM micrograph of the AG9N6 (23.3 wt% N) oxynitride (the length of the reference line is equivalent to 100 nm).

This synthesis method allows high surface area solids to be obtained. The $Al_{0.5}Ga_{0.5}PO_4$ phosphate used as a precursor in this study (AG9), for instance, has a surface area of 240 m^2/g. A TEM analysis of the sample morphology reveals that the solid is constituted by particles of about 10 nm in diameter (see Fig. 2).

The nitrided samples are also characterized by type IV N_2 adsorption and desorption isotherms and, as can be seen in Fig. 3, TEM shows a high morphological similarity with the phosphate precursor.

III.C. Electron Energy Loss Spectroscopy

Information about the type of bonding around anion atoms can be deduced from a detailed analysis of the ELNES.

Figure 4 displays the N–K edge from the most nitrided sample AG9N6 (23.3 wt% N) and those from AlN, GaN, and PON references. Under the dipole selection rule, the N–K edge probes the p-like unoccupied density states (DOS). The large peak extending from 398 to about 404 eV in AG9N6 reveals a structure that is initially reminiscent of the triplet structure characteristic of h-AlN, already interpreted using LMTO, DOS, and MS calculations (45). One can consider the modifications to this picture: the increase in the second peak at 403 eV and the damping of the third peak at 405 eV in relation to the N–K ELNES both in h-GaN, the feature of which is coherent with previous NEXAFS studies (46, 47), and in PON, suggesting that h-GaN, h-AlN, and PON local environments may partly co-exist around nitrogen atoms. Otherwise, the broad peak at about 423 eV is assigned to a shape resonance (48); its position follows the Natoli rule and is related to the first interatomic distances (49). In spite of the slight possible influence of the second neighbor shell made of both nitrogen and oxygen atoms, which needs simulations to be accurately identified, these features confirm the hybrid environment around nitrogen atoms, made of Ga, Al, and P atoms.

Upon long-enough beam exposure time (more than a few minutes) a noticeable rise in the first peak intensity is observed at the N–K threshold onset for AG9N6, as shown in Fig. 5. This phenomenon is spectacularly enhanced for AlPON and PON (not shown) compounds. It can clearly be interpreted as caused by a molecular nitrogen release when features are compared to N–K edge in N_2 gas. Such a release has already been observed for oxygen-doped h-AlN (45). Note that in our case the beam sensitivity only concerns nitrogen, oxygen–K ELNES remaining quite constant

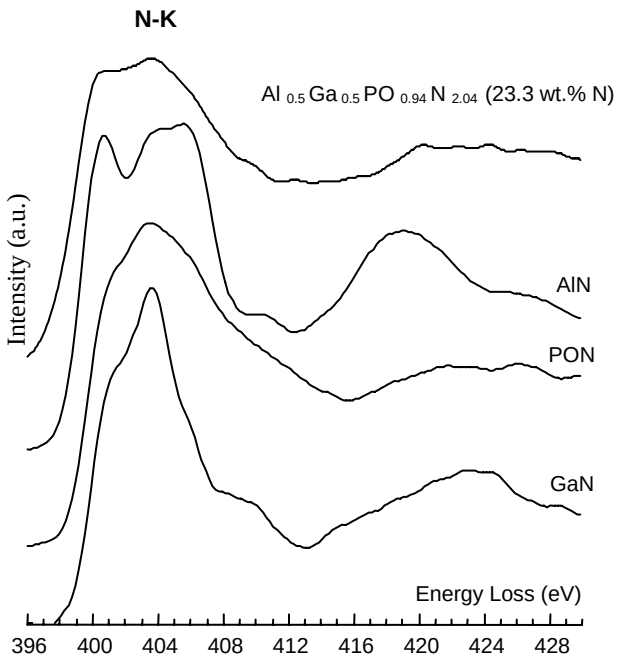

FIG. 4. N–K edge in AG9N6 (23.3 wt% N) oxynitride compared to crystalline references: AlN, PON, and GaN. Spectra were deconvoluted from thickness effects according to the procedure described in Ref. (50).

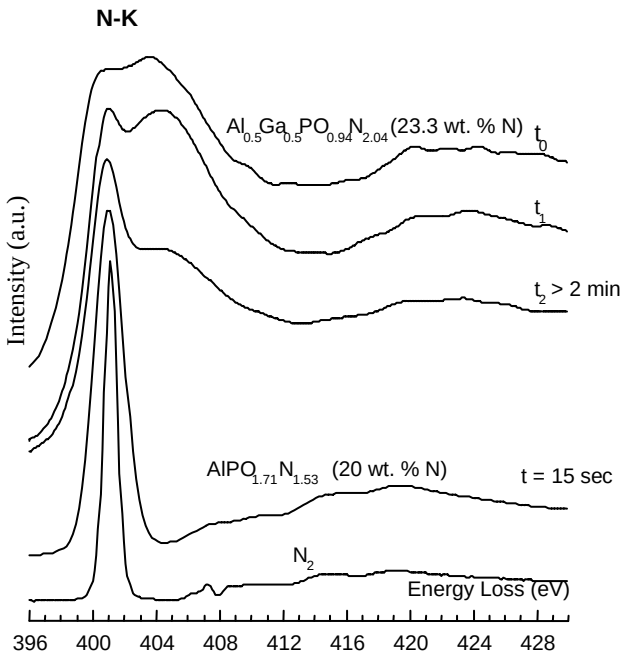

FIG. 5. Evolution of the N–K edge in the AG9N6 (23.3 wt% N) oxynitride during beam exposure. N–K edges in an AlPON oxynitride and in molecular N_2 are also shown. Spectra were deconvoluted from thickness effects according to the procedure described in Ref. (50).

whatever both the exposure time and the nitrogen content (included 0% N).

The quantitative EELS analysis, the [Al]/[Ga] and [Al]/[P] (and [O]/[N]) atomic ratios were measured on different zones of the oxide precursor AG9 and of the oxynitride AG9N6 (23.3 wt% N). The results are presented in Tables 2 and 3, respectively. The [Al]/[Ga] intensity ratios were determined using Hartree–Slater cross sections corrected for a sensitivity factor (generally named *k*-factor), evaluated from the AG9 sample taken as a reference (50). As indicated in Tables 2 and 3, thicknesses of the areas analyzed were of the same order.

TABLE 2
Values of the [Al]/[P] and [Al]/[Ga] Atomic Ratios on the AG9 Oxide Precursor

Probe diameter (nm)	Reduced thickness (t/λ)	[Al]/[P]	[Al]/[Ga]
75	0.247	0.47	1.05
75	0.239	0.56	1.10
27.5		0.50	1.00
27.5		0.47	0.93
27.5	0.239	0.42	1.00
27.5		0.56	0.99
27.5		0.58	0.96
27.5	0.230	0.56	0.93
27.5		0.41	0.99
27.5	0.129	0.49	1.11
27.5		0.42	0.86

Note. The electron mean free path λ is of about 140 nm in our experiments.

TABLE 3
Values of the [Al]/[P], [Al]/[Ga], and [O]/[N] Atomic Ratios on the AG9N6 (23.3 wt% N) Oxynitride

Probe diameter (nm)	Reduced thickness (t/λ)	[Al]/[P]	[Al]/[Ga]	[O]/[N]
27.5	0.099	0.90	1.37	1.51
75	0.153	0.56	0.83	
75	0.234	0.61	0.78	0.83
75	0.276		1.22	
75	0.218			1.24
105				1.11
105	0.165			0.93
105				1.13

Note. The electron mean free path λ is of about 140 nm in our experiments.

The AG9 precursor is homogeneous at the used probe scale: the [Al]/[P]and [Al]/[Ga] relative concentrations slightly vary from one analyzed zone to the other. However, the [Al]/[P] and [Al]/[Ga] atomic ratios measured in diverse zones of the AG9N6 oxynitride are different from the expected values, which is a strong indication that the homogeneity of the material has been lost during nitridation.

The [O]/[N]ratio also varies significantly throughout the sample. This last observation could be explained at least partially by the fact that nitridation was carried out in a static bed tubular furnace, a type of furnace whose performances are strongly influenced by mass and heat transport processes. Besides, the mean [O]/[N] value (1.13) is higher than the value measured by the Grekov method (0.46). Although the local character of the EELS measurements should not be forgotten, the discrepancy between Grekov and EELS measurements could also be partly explained, despite reduced exposure times and the use of low dose on the sample during the experiment, by the sensitivity of N sites to the electron beam in the EELS measurements (see Fig. 5).

III.D. X-ray Absorption Spectroscopy

III.D.1. XANES

III.D.1.1. Crystalline $Al_{0.5}Ga_{0.5}PO_4$. The crystalline $Al_{0.5}Ga_{0.5}PO_4$ was used as a reference for the investigation of the structural changes induced by nitridation. Because no density of states (DOS) calculation exists for this sample, the electronic band structure of quartz has been considered for

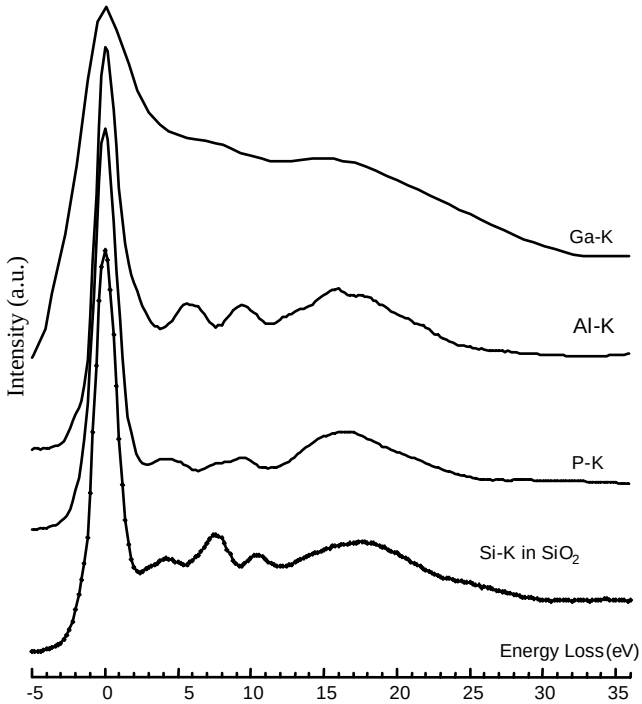

FIG. 6. Comparison of the Ga, Al, and P–K edges in crystalline $Al_{0.5}Ga_{0.5}PO_4$ with Si–K in quartz (SiO_2). For a clear comparison, the spectra have been normalized and aligned on the white line.

comparison. The $Al_{0.5}Ga_{0.5}PO_4$ and SiO_2 are indeed isoelectronic and structurally similar.

Figure 6 displays the P, Al, and Ga–K edges recorded in crystalline $Al_{0.5}Ga_{0.5}PO_4$, compared to the Si–K edge from quartz. A rather satisfying correspondence between the different edges is observed. The raw spectra, consisting of one intense white line (followed by minor fine structures) and one broad resonance, lying at about 16–17 eV beyond the white line, are similar for all four elements. Within the dipole approximation the edges reflect the p local DOS on the cation atom. In SiO_2, the main peak (arbitrary scaled at 0 eV in Fig. 6) is attributed to antibonding cation–oxygen states, while the minor features come from p-t_2 hybridization between the second neighbor cation–cation pairs (51). These structures can also be interpreted as resulting from interferences between the wave functions of an outgoing and multiple backscattered electron waves (52). The broad peak at 17 eV is assigned to a shape resonance arising from the first two shells around the central cation atom (53). The existence of a core hole on the absorber atom in the final state has been shown to have a considerable influence on the shape of the density of empty states, particularly on cation local DOS, which has quasi-atomic character (51). The Ga–K edge differs slightly from the others, its white line being more broadened. This can be partially explained by the difference in the energy resolution (2.5 eV for Ga and an average value of 0.6 eV for Al, P, and Si) and in the core hole width (1.8 eV for Ga, 0.53 eV for P, 0.48 eV for Si, and 0.42 eV for Al) (54).

III.D.1.2. Amorphous $Al_{0.5}Ga_{0.5}PO_4$ and $Al_{0.5}Ga_{0.5}PO_xN_y$. Figures 7, 8, and 9 respectively display the P, Ga, and Al XANES spectra recorded on the AG9 precursor and on the most nitrided sample AG9N6 (23.3 wt% N). The spectra recorded on crystalline references are also shown for comparison.

Some similarities are observed when comparing the P, Ga, and Al–K edges of the crystalline $Al_{0.5}Ga_{0.5}PO_4$ phosphate and of the amorphous AG9 used as a precursor of nitridation in this study: presence of a white line and of a shape resonance (at about 17 eV above the edge), which are the signatures of the X–O_4 tetrahedra (where X = P, Al, or Ga). However, for the three edges, the fine structures located between the white line and the shape resonance, which are observed for the crystalline form, vanish in the spectra of the amorphous one, as an effect of the structural disorder.

Whatever the type of cation, the edges gradually shift toward the lower energy side (the maximum is about 2 eV) as the nitrogen content increases, while an enlargement of the white line is simultaneously visible. This latter is particularly noticeable in the case of the Al–K edge. Both the

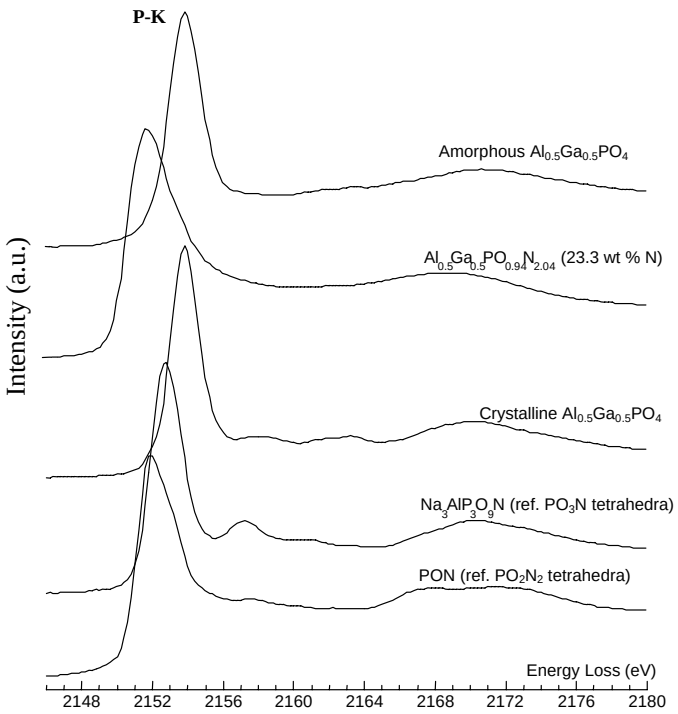

FIG. 7. P–K XANES for the amorphous $Al_{0.5}Ga_{0.5}PO_4$ precursor AG9 and for the nitrided AG9N6 (23.3 wt% N) sample. P–K XANES for crystalline $Al_{0.5}Ga_{0.5}PO_4$, $Na_3AlP_3O_9N$, and PON references are also shown. The spectra were normalized at the maximum of the edge.

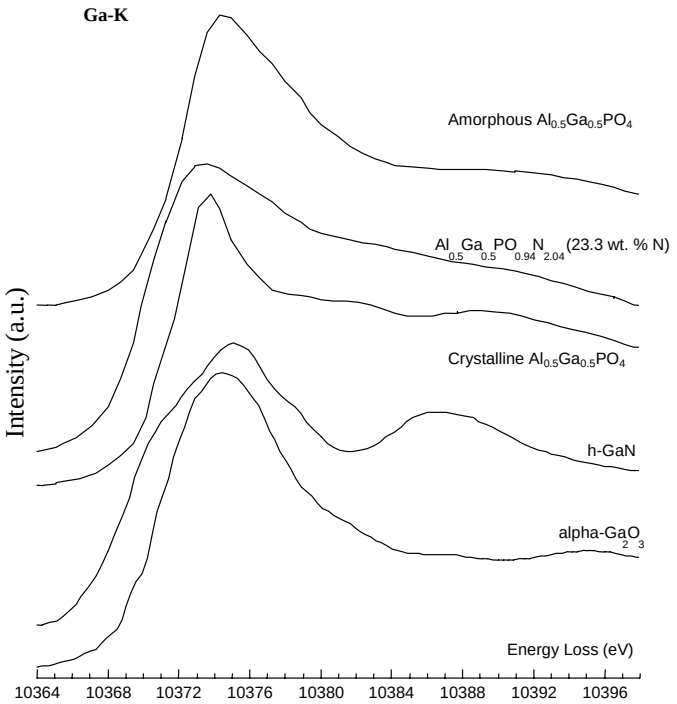

FIG. 8. Ga–K XANES for the amorphous $Al_{0.5}Ga_{0.5}PO_4$ precursor AG9 and for the nitrided AG9N6 (23.3 wt% N) sample. Ga–K XANES for crystalline $Al_{0.5}Ga_{0.5}PO_4$, h-GaN, and α-Ga_2O_3 references are also shown. The spectra were normalized at the maximum of the edge.

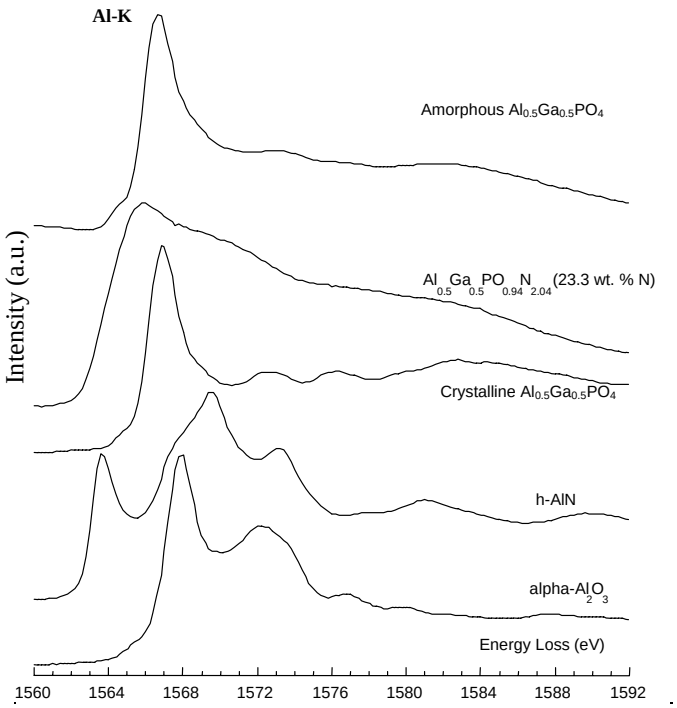

FIG. 9. Al–K XANES for the amorphous $Al_{0.5}Ga_{0.5}PO_4$ precursor AG9 and for the nitrided AG9N6 (23.3 wt% N) sample. Al–K XANES for crystalline $Al_{0.5}Ga_{0.5}PO_4$, h-AlN, and α-Al_2O_3 references are also shown. The spectra were normalized at the maximum of the edge.

TABLE 4
***X*–O and *X*–N Interatomic Distances in Crystalline Compounds**

X–O bonds	Distances (Å)	Ref.	*X*–N bonds	Distances (Å)	Ref.
Ga–O in GaO_4 tetrahedra (in $GaPO_4$)	1.78	55	Ga–N in wurtzite GaN	1.952 1.951	57
Ga–O in GaO_6 octahedra (in α-Ga_2O_3)	1.921 2.077	58			
Al–O in AlO_4 tetrahedra (in $AlPO_4$)	1.70	55	Al–N in wurtzite AlN	1.903 1.889	57
Al–O in AlO_6 octahedra (in α-Al_2O_3)	1.857 1.969	56			
P–O in $Na_3AlP_3O_9N$	1.525 1.522 1.496	6	P–N in $Na_3AlP_3O_9N$	1.707	6
P–O in the low-cristobalite form of $AlPO_4$	1.56	55			
P–O in the low-cristobalite form of $GaPO_4$	1.56	55			
			P–N in $Na_3P_6N_{11}$ (tricoordinated N in PN_4 tetrahedra)	1.73	59
			P–N in $LiPN_2$ (bicoordinated N in PN_4 tetrahedra)	1.64	60

differences in oxygen and nitrogen electronegativities and the fact that the *X*–N distances are longer than the *X*–O ones (*X* being Al (55–57) or Ga (55, 57, 58), or P (6, 55, 59, 60) (see Table 4)) may play a role in the evolution of the XANES (61).

The P–K XANES spectrum recorded on the AG9N6 oxynitride is compared to those from crystalline references: $Na_3AlP_3O_9N$ nitrided phosphate, reference for PO_3N tetrahedra (6, 32–34) and PON nitrided phosphate, reference for PO_2N_2 tetrahedra (35, 36). No reference compounds containing PON_3 tetrahedra were used because, according to Day (62) and Reidmeyer (63), there are no stable nitrided phosphate glasses known to contain such groups.

The P–K threshold energy position of the most nitrided sample AG9N6 is close to the one of the PON sample, which suggests that this sample is mainly constituted of PO_2N_2 tetrahedra.

One has to emphasize that neither the Ga–K nor the Al–K edge position coincides with that observed for commercial GaN at 10,369 eV or AlN at 1563.2 eV during nitrogen incorporation, while they are strongly shifted from

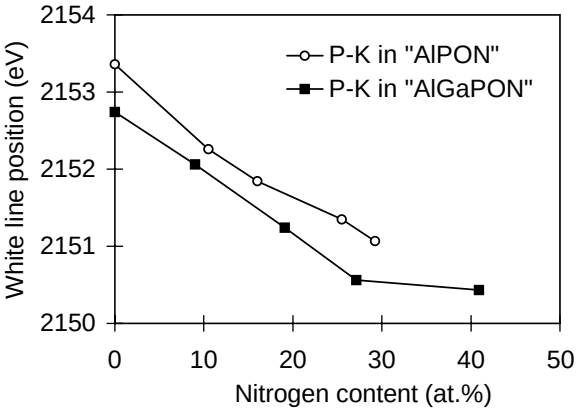

FIG. 10. Variation of the P white line position with the nitrogen enrichment for the AlGaPON and AlPON series of samples.

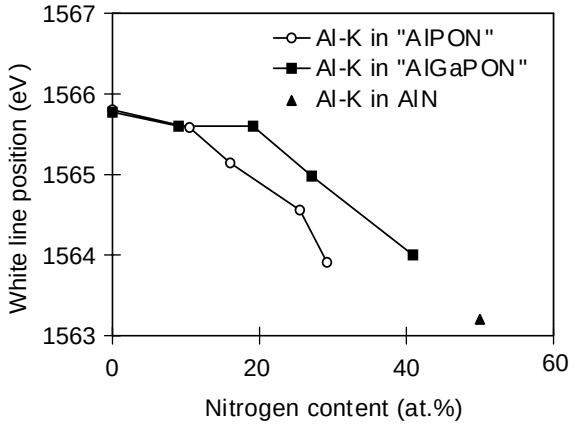

FIG. 12. Variation of the Al white line position with the nitrogen enrichment for the AlGaPON and AlPON series of samples. White line position in crystalline AlN is also shown.

those corresponding to an octahedral environment (α-Al_2O_3 and α-Ga_2O_3).

Figures 10, 11, and 12 respectively present the change of the P, Ga, and Al white line position with the nitrogen enrichment for the AlGaPON series. The error on the exact determination of the white line position is approximately 0.2 eV for Al and P and 0.3 for Ga.

The P–K and Ga–K edges gradually shift toward lower energies as the nitrogen content increases. The position of the Al–K edge is not affected at the beginning of nitridation but shifts toward lower energies when the nitrogen content attains 20 at.%.

The evolution of the P and Al white line position for a series of five AlPON samples, whose synthesis and physico-chemical properties were described in Ref. (64), are also presented in Figs. 10 and 12, respectively. The nitrogen contents must be expressed as at.% for the comparison of the AlPON and AlGaPON series.

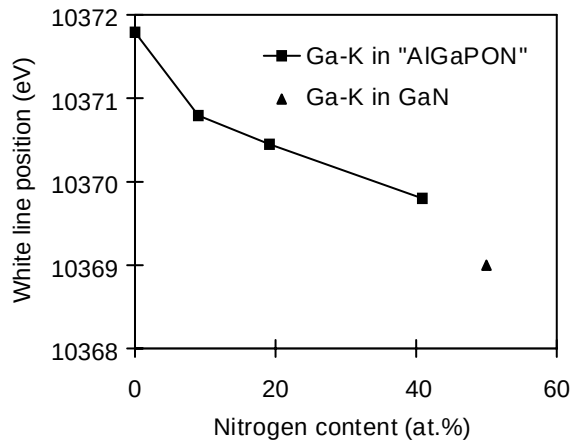

FIG. 11. Variation of the Ga white line position with the nitrogen enrichment for the AlGaPON series of samples. White line position in crystalline GaN is also shown.

In this case also, only the position of the P–K edge is affected at the beginning of nitridation. The Al–K edge shift only becomes significant for nitrogen contents higher than 10.5 at.%.

The two curves presenting the evolution of the position of the P–K edge with the nitrogen enrichment (Fig. 10) are shifted by approximately 0.7 eV. This could be attributed to a second neighbor effect. In contrast, the position of the Al–K edge in the two $AlPO_4$ and $Al_{0.5}Ga_{0.5}PO_4$ are similar, the second neighbour of aluminium atoms being phosphorus atoms in both cases (Fig. 12).

III.D.2. EXAFS

EXAFS analysis was performed on the Ga–K edges recorded in transmission mode for the AlGaPON system. The EXAFS oscillations have been extracted from the experimental spectra using a fifth-order polynomial law to model the atomic absorption beyond the edge with a Lengeler normalization. Fourier transform in R space of the k^3 weighted oscillations was calculated over the energy range 2.5–13.5 $Å^{-1}$. We used a classical fitting procedure to extract the parameters of the first-coordination shell of gallium atoms, where Ga–O and Ga–N experimental phases and amplitudes were respectively extracted from the $GaPO_4$ (four neighbors at 1.786 Å) and GaN (four neighbors at 1.95 Å), with the total coordination number around Ga atoms fixed at four. This starting hypothesis is in agreement with the shape of the XANES Ga edge, as has been discussed above. The analyses have been processed using the same parameters for all the samples and the references.

Figure 13 displays the modulus and the imaginary part of the radial distribution function as extracted from the experiment for the $Al_{0.5}Ga_{0.5}PO_{0.94}N_{2.04}$ (23.3 wt% N) (i.e.,

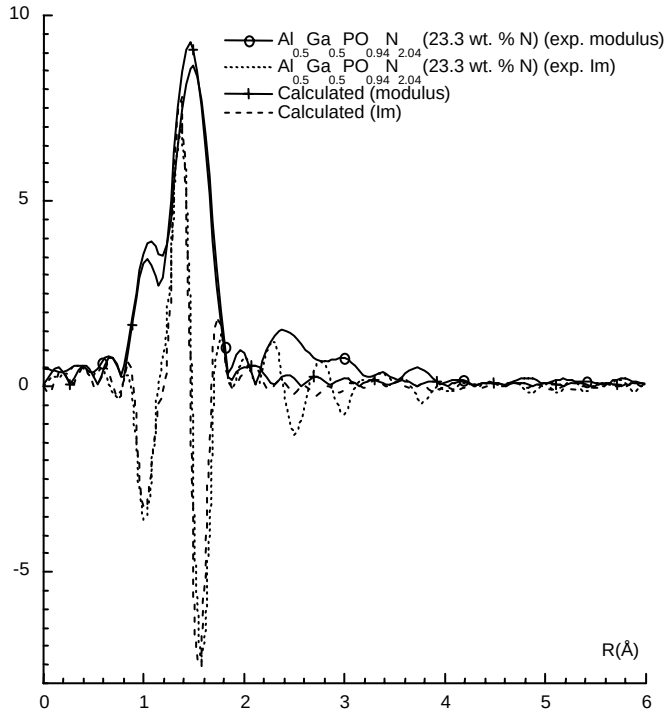

FIG. 13. Fourier transform of the experimental and calculated $k^3 \cdot \chi(k)$ signals for AG9N6 (23.3 wt% N).

AG9N6). The shape of the experimental Fourier transform EXAFS signal confirms the amorphous structure of the powders since one main shell is clearly present, followed by strongly damped peaks corresponding to further shells. So we focused our attention on extracting quantitative information from the first and intense peak, without any attempt to explain medium range order. From the fitting procedure on the experimental spectra, distances and coordination number are deduced. They are gathered in Table 5, together with the results obtained for the other AlGaPON samples. As the difference in phase and amplitude between nitrogen and oxygen is small, the distinction between Ga–N and Ga–O is supported by the significant difference in the distances, as expected from crystalline samples (see Table 4). From the results displayed in Table 5, one can observed that the Ga–O and Ga–N interatomic distances appear constant during nitridation. The values obtained for the different pairs compare well with the crystalline model values. The main change concerns the coordination number and the ratio N(Ga–N)/N(Ga–O). The Ga environment is affected by the nitridation as soon as it starts, while the Ga environment is saturated in nitrogen for a concentration of about 15–16 wt% N.

TABLE 5
Ga–O and Ga–N Distances (R(Å)) and Their Associated Coordination Number (N) for the Different Oxynitrides, Deduced from the Fitting of the Experimental EXAFS Signal (the Corresponding Fit for AG9N6 is Illustrated in Fig. 13)

Sample	wt % N content	Ga–O		Ga–N	
		R(Å) $\pm$ 0.02	$N \pm 10\%$	R(Å) $\pm$ 0.02	$N \pm 10\%$
AG9N2	5.3	1.82	3	1.96	1
AG9N4	11	1.82	2.9	1.97	1.1
AG9N5	15.9	1.82	2.4	1.97	1.6
AG9N6	23.3	1.815	2.5	1.96	1.5

Al and P–K edges, which were recorded in Total Electron Yield mode, were not of sufficient quality to allow such a treatment to be done. Explanations for that could be related to possible charge effects.

III.E. X-ray Photoelectron Spectroscopy

XPS spectra contain two types of peaks: photoelectric peaks and Auger peaks. For the first, one speaks of the electron binding energies; for the second, the concept of kinetic energies is more adequate. Indeed, the kinetic energy of an Auger electron is independent of the X-ray source energy. Hence, by modifying the source energy, one can modify the relative positions of Auger and photoelectric peaks. This concept has to be used to study the AlGaPON oxynitrides. Indeed, one characteristic of XPS gallium spectra is the presence of numerous Auger peaks in the region of kinetic energies varying from 830 to 1254 eV (65).
—With the aluminium anode (Al$K\alpha_{1,2}$:$h\nu$ 1486.6 eV), the N_{1s} photoelectric peak is superposed to a Ga Auger peak (66), which complicates the determination of the superficial nitrogen atomic concentration;
—With the magnesium anode (Mg$K\alpha_{1,2}$:$h\nu$ 1253.6 eV), the C_{1s} photoelectric peak is superposed to a Ga Auger peak (66, 67), which impedes the exact determination of the C–(C, H) component of the adventitious carbon (65).

Hence, we combined data obtained with both Al and Mg anodes.

The XPS spectrum of the N_{1s} electrons recorded on the less nitrided sample (AG9N2—5.3 wt% N) and that of a highly nitrided sample (AG9N5—15.9 wt% N) are presented in Fig. 14. They were recorded with a non-monochromatized Mg anode to avoid the N_{1s} and Ga Auger peak superposition.

They are centered around 397.8 eV, i.e., in the binding energy range of N_{1s} electrons in many nitrided samples (68) and in nitrided phosphate glasses in particular (69). In those glasses, the P=N–P bonding configuration gives rise to a N_{1s} XPS peak centered around 397.8 eV and the $\overset{N}{\underset{N}{}} > P–N$ bonding configuration gives rise to a N_{1s} peak centered around 399.3 eV.

In the case of AG9N2 (5.3 wt% N) and AG9N5 (15.9 wt% N), it is not possible to deconvolute the N_{1s} peak and to

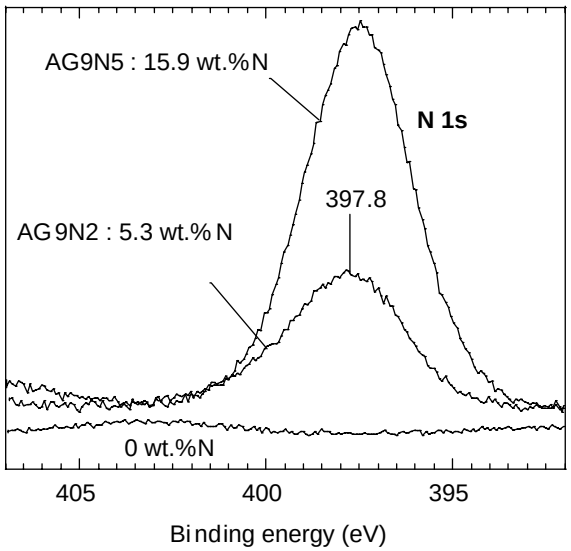

FIG. 14. N_{1s} XPS spectra of AG9, AG9N2 (5.3 wt% N), and AG9N5 (15.9 wt% N).

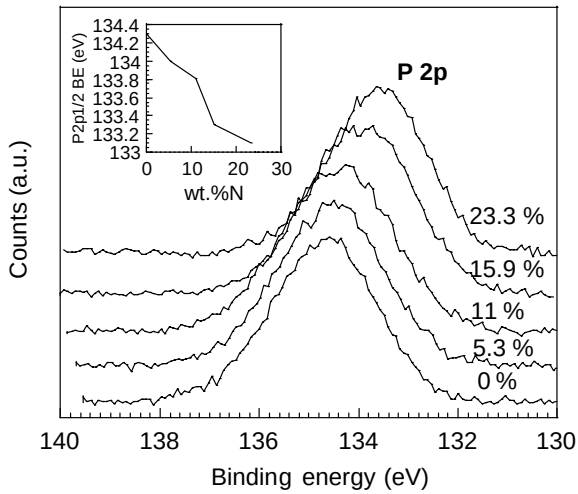

FIG. 16. Variation of the P_{2p} XPS peaks with the nitrogen enrichment (expressed as wt% N) of AlGaPON.

discriminate those two bonding configurations. However, one can consider that the =N– bonding configuration is dominant. Indeed, Reidmeyer *et al.*, in a structural model for nitrogen incorporation in phosphate glasses, predict that three =N– species are formed for every >N– species (63, 70).

The surface nitrogen concentrations evaluated from the areas of the XPS peaks on the AlGaPON series of samples were compared to those predicted from the Grekov chemical analysis for the bulk nitrogen concentrations (Fig. 15). There is reasonable agreement between the two sets of data. Surface reoxidation or the presence of residual adsorbed water explains that, for some samples, the surface nitrogen concentration is slightly lower than the bulk nitrogen content.

The variation of the P_{2p}, Ga_{3d}, and Al_{2p} peaks with the nitrogen enrichment is presented in Figs. 16, 17, and 18, respectively. The spectra were recorded using the monochromatized aluminium anode. The position of all three peaks—as well as those of the Ga_{3p} peaks (not shown)—shifts to lower binding energies as the nitrogen content of the sample increases. However, for the Al_{2p} peaks, the binding energy decrease is not significant (< 0.2 eV) for nitrogen contents less than 11 wt%.

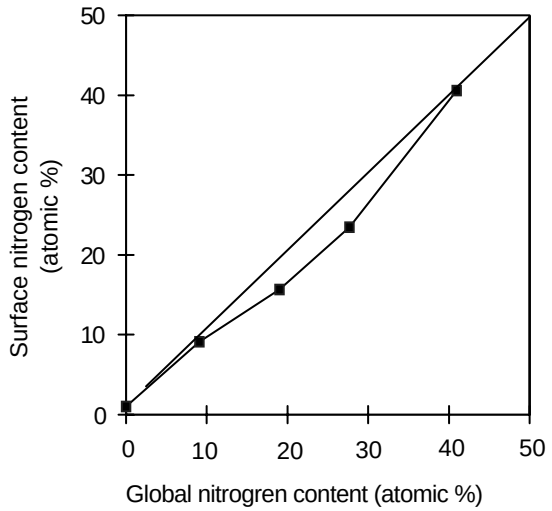

FIG. 15. Variation of the surface nitrogen content with the global nitrogen content.

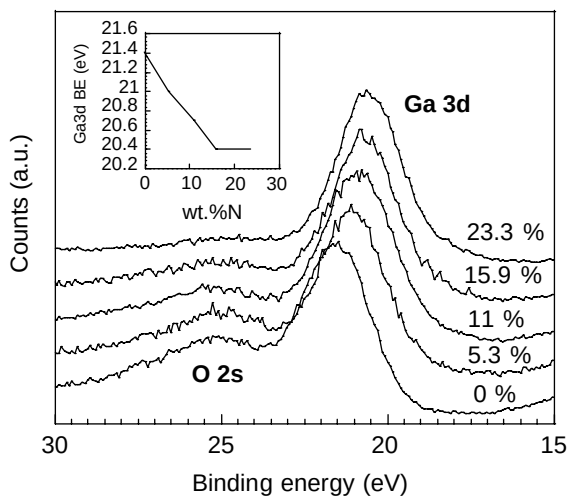

FIG. 17. Variation of the Ga_{3d} XPS peaks with the nitrogen enrichment (expressed as wt% N) of AlGaPON.

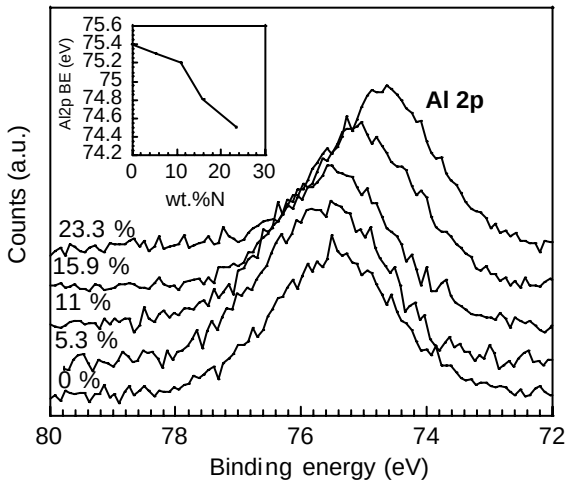

FIG. 18. Variation of the Al_{2p} XPS peaks with the nitrogen enrichment (expressed as wt% N) of AlGaPON.

The P_{2p}, Ga_{3d}, and Al_{2p} binding energy decrease observed upon O/N substitution could be explained by the stronger nucleophilic character of nitrogen as compared to oxygen, which reduces the positive charge around those atoms. Changes in the binding energies of P_{2p}, Ga_{3d}, and Al_{2p} electrons were already described when comparing P–O bonds and P–N bonds in nitrided alkali metaphosphate glasses (71), Ga–O bonds and Ga–N bonds in oxidized GaN (67), and also Al–O bonds and Al–N bonds in oxygen-contaminated AlN (72).

IV. DISCUSSION

IV.1. The Phosphate Precursor

The $Al_{0.5}Ga_{0.5}PO_4$ phosphate precursor synthesized by a method developed by Kearby (31) is an X-ray amorphous white powder with a homogeneous texture (Fig. 2). The quantitative EELS analysis of the [Al]/[Ga] and [Al]/[P] atomic ratios for the precursor demonstrate that its composition is homogeneous at the probe scale used, while XANES (Fig. 6 compared to Figs. 7–9) suggests that the SiO_2-like structure is preserved in the first shells.

Moreover, as stated in Ref. (13), differential thermal analysis reveals that the $Al_{0.5}Ga_{0.5}PO_4$ gives rise to only one crystallization peak, at 955°C, when heated at 10°C min^{-1}, whereas $AlPO_4$ and $GaPO_4$ crystallize at 1120 and 775°C, respectively, under the same experimental conditions. This allows us to consider $Al_{0.5}Ga_{0.5}PO_4$ as a true solid solution, rather than a mixture of $AlPO_4$ and $GaPO_4$.

However, ^{31}P nuclear magnetic resonance experiments reveal the presence of a randomized distribution of $P(OAl_{4-x}Ga_x)$ sites rather than of a single $P(OAl_2Ga_2)$ type of site around phosphorus atoms in the $Al_{0.5}Ga_{0.5}PO_4$ precursor (73).

IV.2. The Nitrided "AlGaPON"

The nitridation mechanism of the $Al_{0.5}Ga_{0.5}PO_4$ precursor has been previously investigated by performing its ammonolysis "*in situ*" in a DRIFTS cell. This study allowed us to propose the following nitridation mechanism (74).

At first, ammonia adsorbs on the surface by reacting with the Brönsted –OH acid sites and the Lewis acid sites. Then, ammonia substitutes the terminal hydroxyl groups to form $-NH_2$ amino groups. In a third step, imido –NH– species are formed, either by condensation of two $M-NH_2$ groups or by condensation of an amine with another hydroxyl group. Finally, nitridation of the solid network occurs, nitrogen incorporation in the bulk phase being ensured by diffusion.

Nitrogen incorporation in the $Al_{0.5}Ga_{0.5}PO_4$ precursor is favored by (I) its high surface area (240 m^2/g), maximizing the reaction area and minimizing diffusion distances and (II) its amorphous nature. Indeed, in the bulk phase, diffusion rates are generally much greater for amorphous materials than for their crystalline counterparts (75).

Nitridation induces a reduction of the surface area of approximately 35%. This reduction mostly takes place at the beginning of nitridation, and then the surface area is not significantly affected by the time of nitridation (see Table 1). It is however noticeable that the surface area remains above 140 m^2/g despite long treatments (maximum 89 h) under ammonia at high temperature (750°C) accompanied by a chemical composition modification and the production of water. Those high surface areas are essential for future applications of AlGaPON as heterogeneous catalysts.

The effective diffusion of nitrogen in the bulk phase was proposed in Ref. (76). Figure 15, showing the correspondence between the surface and the bulk nitrogen concentrations, illustrates this phenomenon.

Several indications lead us to think that the first-coordination spheres of all three P, Ga, and Al atoms are affected by the O/N substitution:

1. ELNES experiments indicate a hybrid environment around nitrogen atoms, made of P, Ga, and Al atoms (Fig. 4);

2. The P_{2p}, Ga_{3d}, and Al_{2p} electron binding energies measured by XPS (Figs. 16–18) decrease when nitrogen is incorporated in the network, which is consistent with the substitution of oxygen for nitrogen in the first-coordination sphere of those cations;

3. The P, Ga, and Al XANES spectra (Figs. 7–9) recorded on oxynitrides are significantly different from those recorded on the phosphate precursor: their threshold energy positions are shifted toward the lower energy side and the white lines are broadened with the nitrogen enrichment, as would be expected if oxygen was substituted for nitrogen.

By comparing the P–K XANES spectra recorded on the most nitrided sample AG9N6 (23.3 wt% N) and those

recorded on the $Na_3AlP_3O_9N$ (reference for PO_3N units) and on the PON (reference for PO_2N_2 units) crystalline samples, we concluded that PO_2N_2 tetrahedra mainly constitute the AG9N6 oxynitride. Similar conclusions were obtained by Benitez *et al.* (25) on the AlPON system. These authors combined X-ray photoelectron spectroscopy (XPS) with mass spectrometry temperature-programmed desorption (TPD-MS) experiments on amorphous $AlPO_4$ and six nitrided aluminophosphates AlPON. They concluded that PO_3N tetrahedra were preferentially obtained at the beginning of nitridation, and then, in a second nitridation stage, PO_2N_2 units were formed when the nitrogen content becomes greater than 11 wt%.

Hence, ELNES, XPS, and XANES spectroscopies lead us to believe that, in AlGaPON, the oxygen atoms located in the first-coordination sphere of aluminium, gallium, and phosphorus atoms can be substituted for nitrogen.

Nitridation, however, may induce a loss of homogeneity of the material: the [Al]/[Ga], [Al]/[P], and [O]/[N] atomic ratios evalutated by EELS spectroscopy on the most nitrided sample AG9N6 (23.3 wt% N) vary significantly from one analyzed zone to the other (Table 3). For this sample, discrepancies between bulk [Al]/[Ga]and [Al]/[P] atomic ratios and the superficial atomic ratios evaluated by XPS had already been underlined (76).

As was already suggested on the AlPON oxynitrides, we propose that the substitution of the oxygen atoms located in the first-coordination sphere of aluminium by nitrogen atoms is not favored and does not take place at the beginning of nitridation: (I) the position of the Al–K edge is not affected at the beginning of nitridation and the shift of this edge only becomes significant for nitrogen contents higher than 11 wt% (19 at.% N) (Fig. 12); (II) the Al_{2p} electron binding energy decrease only occurs for nitrogen contents higher than 11 wt% (Fig. 18).

In the contrast, nitrogen is preferentially incorporated in the first atomic shell of gallium atoms as soon as nitridation starts. This is clearly shown by the EXAFS analysis performed on the Ga–K edges of the series of AlGaPON samples. The comparison of the experimental and calculated EXAFS signals (Table 5) shows that, on average, one oxygen atom is substituted by one nitrogen atom in the first-coordination sphere of the gallium atoms in the less nitrided sample AG9N2 (5.3 wt% N). However, those calculations also show that the gallium environment is saturated in nitrogen for concentrations of about 15–16 wt% N. One can parallel this result with the fact that the Ga_{3d} electron binding energies measured by XPS for the two most nitrided samples AG9N5 (15.9 wt% N) and AG9N6 (23.3 wt% N) are similar (Fig. 17).

We thus propose that Ga–O–P bonds are replaced by Ga–N–P bonds preferentially to Al–O–P bonds. Or, in other words, that gallium favors incorporation of nitrogen in the phosphate network. This assumption is supported by two experimental observations:

1. During ELNES analysis, molecular nitrogen release upon exposure of oxynitrides under the electron beam is spectacularly reduced for AlGaPON as compared to AlPON (Fig. 5);

2. The substitution of aluminium atoms by gallium atoms in the precursor favors nitrogen incorporation during nitridation (13):

—The minimum nitridation temperature decreases when the gallium content of the sample increases. For instance, the minimum nitridation temperature of an $AlPO_4$ oxide is approximately 600°C while the minimum nitridation temperature of a $GaPO_4$ oxide is approximately 400°C;

—The amount of nitrogen incorporated in the phosphate structure under fixed reaction conditions increases with the gallium enrichment of the samples.

To explain the influence of gallium, we considered thermodynamic factors. As no thermodynamic data concerning the ammonolysis of $AlPO_4$ or $GaPO_4$ to AlPON and GaPON existed, we approached the problem by comparing the free energy of reaction values to produce AlN and GaN by nitridation under ammonia of Al_2O_3 and Ga_2O_3 (Table 6). Thermodynamic data were taken from Ref. (77). The results show that the formation of GaN from Ga_2O_3 is more favorable around 750°C than the formation of AlN from Al_2O_3.

Balkas *et al.* (78) have studied various GaN synthesis routes, among which the reaction of Ga_2O_3 with ammonia. This reaction occurs in the 600–1000°C temperature range (79). The authors note that the nitridation occurs in two steps: the reduction of Ga_2O_3 to Ga_2O in the presence of H_2, NH, or NH_2 and the subsequent synthesis of GaN by reaction of Ga_2O with ammonia, this second reaction being thermodynamically favored. If reduction of gallium also occurs during the nitridation of the $Al_{0.5}Ga_{0.5}PO_4$ precursor, it could accelerate the rate of the nitridation reaction, provided that it decreases the activation energy of the nitridation rate-limiting step.

TABLE 6

Free Energy of Reaction Values To Produce AlN and GaN by Nitridation under Ammonia of Al_2O_3 and Ga_2O_3 at 727°C (1000 K)

Reaction	Free energy of the reaction (ΔG_r (kJ/mol))
$Al_2O_3(s) + 2NH_3(g) \rightarrow 2AlN(s) + 3H_2O(g)$	236
$Ga_2O_3(s) + 2NH_3(g) \rightarrow 2GaN(s) + 3H_2O(g)$	80

Note. The free energies of formation of Al_2O_3 (-1361.331 kJ/mol), Ga_2O_3 (-762.258 kJ/mol), AlN (-211.799 kJ/mol), and GaN (9.920 kJ/mol) at 727°C (1000 K) were taken from Ref. (77).

V. CONCLUSIONS

The changes induced by nitridation on the short range structure of an amorphous $Al_{0.5}Ga_{0.5}PO_4$ precursor were investigated. Three spectroscopies sensitive to the local environment of atoms in solids, namely, electron energy loss spectroscopy (EELS), X-ray absorption spectroscopy (XAS), and X-ray photoelectron spectroscopy (XPS) were used to answer the two questions formulated in the Introduction.

Those questions arose from results obtained on AlPON catalysts: on those solids, it has been shown that phosphorus atoms are nitrided preferentially to aluminium atoms and that the nitridation induces the segregation of two phases: an Al_2O_3-like phase and (–N=P–N=) cyclic arrangements (24).

The results presented in this paper suggest that, for the AlGaPON system, nitrogen is incorporated in the first-coordination sphere of P, Al, and Ga atoms. However, the substitution of nitrogen in the first-coordination sphere of Al is probably not favored as compared to nitrogen incorporation around P or Ga atoms. We thus propose that Ga–O–P bonds are replaced by Ga–N–P bonds preferentially to Al–O–P bonds at the beginning of nitridation (below incorporation of 11 wt% N). This conclusion is also supported by a previous study of the kinetics of nitridation of amorphous $Al_{1-x}Ga_xPO_4$ phosphates that had shown that the substitution of aluminium by gallium in the precursor facilitated nitrogen incorporation in the network (13).

ACKNOWLEDGMENTS

The authors thank M. Roger Marchand ("Laboratoire de Chimie des Matériaux" (Université de Rennes I, France)) for delivering reference samples with mixed PO_xN_y tetraheda and data about them. They are grateful to Michel Genet (Université catholique de Louvain, Belgique) for the help provided in the recording and processing of XPS spectra. They would also like to thank the "Fonds National de la Recherche Scientifique (FNRS)" for the fellowship awarded to Miss Stéphanie Delsarte.

REFERENCES

1. K. Tanabe, M. Misono, Y. Ono, and H. Hattori, *in* "Studies in Surface Science and Catalysis 51, New solid acids and bases," p. 188. Elsevier, Amsterdam, 1989.
2. J. M. Campelo, A. Garcia, J. M. Gutierrez, D. Luna, and J. M. Marinas, *Can. J. Chem.* **61,** 2567 (1983).
3. J. M. Campelo, A. Garcia, J. M. Gutierrez, D. Luna, and J. M. Marinas, *J. Colloid Interface Sci.* **95**(2), 544 (1983).
4. J. B. Moffat, *Catal. Rev.-Sci. Eng.* **18**(2), 199 (1978).
5. R. Marchand, R. Conanec, Y. Laurent, P. Bastians, P. Grange, L. Gandia, M. Montes, J. Fernandez, J. A. Odriozola, and J. Razafindrakoto, Patent WO9521123.
6. R. Conanec, Ph.D. thesis, Université de Rennes I, 1994.
7. N. Fripiat and P. Grange, *J. Chem. Soc. Chem. Commun.* 1409 (1996).
8. N. Fripiat, R. Conanec, R. Marchand, Y. Laurent, and P. Grange, *J. Eur. Ceram. Soc.* **17,** 2011 (1997).
9. N. Fripiat, R. Conanec, A. Auroux, Y. Laurent, and P. Grange, *J. Catal.* **167,** 543 (1997).
10. N. Fripiat, V. Parvulescu, V. I. Parvulescu, and P. Grange, *Appl. Catal. A* **181,** 331 (1999).
11. P. Grange, P. Bastians, R. Conanec, R. Marchand, and Y. Laurent, *Appl. Catal. A* **114,** L191 (1994).
12. P. Grange, P. Bastians, R. Conanec, R. Marchand, Y. Laurent, L. Gandia, M. Montes, and J. A. Odriozola, *in* "Studies in Surface Science and Catalysis-91, Preparation of catalysts VI" (G. Poncelet *et al.*, Eds.), p. 381. Elsevier, Amsterdam, 1995.
13. V. Peltier, R. Conanec, R. Marchand, Y. Laurent, S. Delsarte, E. Guéguen, and P. Grange, *Mater. Sci. Eng. B* **47**(2), 177 (1997).
14. S. Delsarte, V. Peltier, Y. Laurent, and P. Grange, *in* "Studies in Surface Science and Catalysis 118, Preparation of catalysts VII" (B. Delmon *et al.*, Eds.), pp. 869–878. Elsevier, Amsterdam, 1998.
15. S. Delsarte, Ph.D. Thesis, Université catholique de Louvain, 2000.
16. S. Delsarte, A. Auroux, and P. Grange, *Phys. Chem. Chem. Phys.* **2,** 2821 (2000).
17. S. Delsarte, F. Maugé, J.C. Lavalley, and P. Grange, *Catal. Lett.* **68,** 79 (2000).
18. J. March, *in* "Advanced Organic Chemistry, Reactions, Mechanisms and Structure, 4th Ed." p. 945. Wiley/Interscience, New York, 1992.
19. E. Guéguen, S. Delsarte, V. Peltier, R. Conanec, R. Marchand, Y. Laurent, and P. Grange, *J. Eur. Ceram. Soc.* **17,** 2007 (1997).
20. S. Delsarte, Y. Laurent, and P. Grange, *in* "Materials Science Forum 325–326, Nitrides and Oxynitrides" (S. Hampshire and M. J. Pomeroy, Eds.), p. 51. Trans Tech Publications, Switzerland, 2000.
21. A. Marquez, J. F. Sanz, and J. A. Odriozola, *J. Non Cryst. Solids*, **263–264,** 189 (2000).
22. T. Blasco, A. Corma, L. Fernandez, V. Fornez, and R. Guil-Lopez, *Phys. Chem. Chem. Phys.* **1,** 4493 (1999).
23. J. J. Benitez, J. A. Odriozola, R. Marchand, Y. Laurent, and P. Grange, *J. Chem. Soc. Faraday Trans.* **91**(24), 4477 (1995).
24. J. J. Benitez, A. Diaz, Y. Laurent, and J. A. Odriozola, *J. Mater. Chem.* **8**(3), 687 (1998).
25. J. J. Benitez, A. Diaz, Y. Laurent, and J. A. Odriozola, *Appl. Catal. A* **176,** 177 (1999).
26. J. J. Benitez, A. Diaz, Y. Laurent, P. Grange, and J. A. Odriozola, *Z. Phys. Chem. Int.* **202,** 21 (1997).
27. A. Diaz, J. J. Benitez, Y. Laurent, and J. A. Odriozola, *J. Non-Cryst. Solids* **238,** 163 (1998).
28. A. Marquez, J. F. Sanz, J. J. Benitez, M. A. Centeno, and J. A. Odriozola, *J. Phys. Chem. B* **103,** 10850 (1999).
29. A. Stein, B. Wehrle, and M. Jansen, *Zeolites* **13,** 291 (1993).
30. R. C. Weast and M. J. Aslte, Eds. *in* "CRC Handbook of Chemistry and Physics–61st ed." CRC Press, Boca Raton, FL, 1980.
31. K. Kearby, *in* "Proceedings, 2nd International Congress on Catalysis, Paris, 1960," p. 2567. Technip, Paris, 1961.
32. R. Conanec, P. L'Haridon, W. Feldmann, R. Marchand, and Y. Laurent, *Eur. J. Solid State Inorg. Chem.* **31,** 13 (1994).
33. R. Conanec, W. Feldmann, R. Marchand, and Y. Laurent, *J. Solid State Chem.* **121,** 418 (1996).
34. D. Massiot, R. Conanec, W. Feldmann, R. Marchand, and Y. Laurent, *Inorg. Chem.* **35,** 4957 (1996).
35. R. Marchand and Y. Laurent, *Eur. J. Solid. State Inorg. Chem.* **28,** 57 (1991).
36. J. M. Léger, J. Hainest, L. S. de Oliveira, C. Chateau, A. Le Sauze, and R. Marchand, *J. Phys. Condens. Matter* **8,** L773 (1996).
37. F. F. Grekov, J. Guyader, R. Marchand, and J. Land, *Rev. Chim. Min.* **15,** 341 (1978).
38. R. F. Egerton, *Ultramicroscopy* **3,** 243 (1978).
39. M. P. Seah, *Surf. Interface Anal.* **2,** 222 (1980).
40. M. T. Anthony and M. P. Seah, *Surf. Interface Anal.* **6,** 95 (1984).
41. R. L. Chaney, *Surf. Interface Anal.* **10,** 36 (1987).

42. L. T. Weng, G. Vereecke, M. J. Genet, P. G. Rouxhet, J. H. Stone-Masui, P. Bertrand, and W. E. Stone, *Surf. Interface Anal.* **20,** 193 (1993).
43. N. Fripiat and P. Grange, *J. Mater. Sci.* **34,** 2057 (1999).
44. S. J. Gregg and K. S. W. Sing *in* "Adsorption, Surface Area and Porosity-2nd Edition," p. 111. Academic Press, San Diego, 1982.
45. V. Serin, C. Colliex, R. Brydson, S. Matar, and F. Boucher, *Phys. Rev. B* **58**(8), 5106 (1998).
46. W. R. L. Lambrecht, S. N. Rashdeev, B. Segall, K. Lawniczak-Jablonska, T. Suski, E. M. Gullikson, J. H. Underwood, R. C. C. Perera, J. C. Rife, I. Grzegory, S. Porowski, and D. K. Wickenden, *Phys. Rev. B*: *Condens. Mater.* **55**(4), 2612 (1997).
47. M. Katsikini, M. Fieber-Erdman, E. Holub-Krappe, D. Korakakis, T. D. Moustakas, and E. C. Paloura, *J. Synchrotron Radiation* **6,** 558 (1999).
48. A. J. Craven, *Microscopy* **180,** 250 (1995).
49. C. R. Natoli, *in* "EXAFS and Near Edge Structure" (L. Incoccia and S. Stipcich, Eds.), p. 43. Springer Series on Chemical Physics, Springer-Verlag, Berlin, New York, 1983.
50. R. F. Egerton, *in* "Electron Energy Loss Spectroscopy in electron microscopy," p. 27. Plenum, New York, 1996.
51. F. Jollet and C. Noguera, *Phys. Status. Solidi.* **179,** 473 (1993).
52. V. Briois, Ph. Sainctavit, and A. M. Flank, *Jpn. J. Appl. Phys.* **32,** 52 (1993).
53. P. Lagarde, A-M. Flank, G. Tourillon, R. C. Liebermann, and J. P. Itié, *J. Phys. I* **2,** 1043 (1992).
54. M. O. Krause and J. H. Oliver, *J. Phys. Chem. Ref. Data* **8**(2), 32 (1979).
55. R. W. G. Wyckoff, *in* "Crystal structures-vol. 3," p. 29. Interscience, New York, 1981.
56. W. Y. Ching and Yong-Nian Xu, *J. Am. Ceram. Soc.* **77**(2), 404 (1994).
57. H. Schultz and K. H. Thiemann, *Solid State Commun.* **23,** 815 (1977).
58. M. Marezio and J. P. Remeika, *J. Chem. Phys.* **46**(5), 1862 (1967).
59. J. Ronis, B. Bondars, A. A. Vitola, and T. Millers, *Latv. PSR Zinat. Akad. Vest. Kim. Ser.* **3,** 299 (1990).
60. R. Marchand, P. L'Haridon, and Y. Laurent, *J. Solid State Chem.* **43,** 126 (1982).
61. D. Z. Von Schwarsenbach, *Kristallografiya* **123,** 161 (1966).
62. D. E. Day, *J. Non Cryst. Solids* **112,** 7 (1989).
63. M. R. Reidmeyer and D. E. Day, *J. Mater. Res.* **6**(8), 1757 (1991).
64. A. Massinon, E. Guéguen, R. Conanec, R. Marchand, Y. Laurent, and P. Grange, *in* "Proceedings, 11th International Congress on Catalysis, Baltimaore, 1996" (J. W. Hightower, W. N. Delgass, E. Iglesea, and A. T. Bell, Eds.), "Studies in Surface Science and Catalysis 40," p. 77. Elsevier, Amsterdam, 1996.
65. "Handbook of Auger Electron Spectroscopy—Physical Electronics Division," p. 105. Eden Prairie, MN, 1976.
66. S. S. Lee, S. M. Park, and P. J. Chong, *J. Mater. Chem.* **3,** 347 (1993).
67. S. D. Wolter, B. P. Luther, D. L. Waltemyer, C. Önneby, S. E. Mohney, and R. J. Molnar, *Appl. Phys. Lett.* **70**(16), 2156 (1997).
68. C. D. Wagner, W. M. Riggs, L. E. Davis, and J. F. Moulder, *in* "Handbook of X-ray Photoelectron Spectroscopy—Physical Electron Division, Perkin-Elmer Corporation" (G. E. Muilenberg, Ed.), 1st ed. Eden Prairie, MN, 1979.
69. R. Marchand, D. Agliz, L. Boukbir, and A. Quemarais, *J. Non Cryst. Solids* **103,** 35 (1988).
70. M. R. Reidmeyer and D. E. Day, *J. Non Cryst. Solids* **181,** 201 (1995).
71. R. K. Brow, M. R. Reidmeyer, and D. E. Day, *J. Non Cryst. Solids* **99,** 178 (1988).
72. J. A. Kovacich, J. Kasperkiewicz, D. Lichtman, and C. R. Aita, *J. Appl. Phys.* **55**(8), 2935 (1984).
73. V. Peltier, Ph.D. thesis, Université de Rennes I, 1997.
74. M. A. Centeno, S. Delsarte, and P. Grange, *J. Phys. Chem. B* **103**(34), 7214 (1999).
75. C. R. Bickmore and R. M. Laine, *J. Am. Ceram. Soc.* **79**(11), 286 (1996).
76. S. Delsarte, V. Peltier, Y. Laurent, and Y. P. Grange, *J. Eur. Ceram. Soc.* **18,** 1287 (1998).
77. I. Barin, *in* "Thermochemical Data of Pure Substances—Part I (Ag–Kr)," pp. 42, 48, 597, 600. VCH, New York, 1993.
78. C. M. Balkas and R. F. Davis, *J. Am. Ceram. Soc.* **79**(9), 2309 (1996).
79. M. R. Lorenz and B. B. Binkowski, *J. Electrochem. Soc.* **109**(1), 24 (1962).